Computers & Geosciences 178 (2023) 105417

Contents lists available at ScienceDirect

Computers and Geosciences

journal homepage: www.elsevier.com/locate/cageo

Probabilistic volcanic mass flow hazard assessment using statistical surrogates of deterministic simulations

Stuart R. Mead *, Jonathan Procter, Mark Bebbington

Volcanic Risk Solutions, School of Agriculture and Environment, Massey University, Palmerston North, New Zealand

ARTICLE INFO

Keywords:
Probabilistic volcano hazard assessment
Numerical modelling
Surrogate modelling
Emulation
Pyroclastic flow

ABSTRACT

Probabilistic volcanic hazard assessments require (1) an identification of the hazardous volcanic source; (2) estimation of the magnitude-frequency relationship for the volcanic process; (3) quantification of the dependence of hazard on magnitude and external conditions; and (4) estimation of hazard exceedance from the magnitude-frequency and hazard intensity relationship. For volcanic mass flows, quantification of the hazard is typically undertaken through the use of computationally expensive mass flow simulators. However, this computational expense restricts the number of samples that can be used to produce a probabilistic assessment and limits the ability to rapidly update hazard assessments in response to changing source probabilities. We develop an alternate approach to defining hazard intensity through a surrogate model that provides a continuous estimate of simulation outputs at negligible computational expense, demonstrated through a probabilistic hazard assessment of dome collapse (block-and-ash) flows at Taranaki volcano, New Zealand. A Gaussian Process emulator trained on a database of simulations is used as the surrogate model of hazard intensity across the input space of possible dome collapse volumes and configurations, which is then sampled using a volume-frequency relationship of dome collapse flows. The demonstrated technique is a tractable solution to the problem of probabilistic volcanic hazard assessment, with the surrogates providing a good approximation of the simulator, and is generally applicable to volcanic hazard and geo-hazard assessments that are limited by the demands of numerical simulations and changing source probabilities.

1. Introduction

Volcanic mass flows such as pyroclastic density currents, lahars, and debris avalanches are amongst the most hazardous volcanic phenomena generated by volcanic eruptions and unrest (Brown et al., 2017). Appropriate management and mitigation of risks to infrastructure and population from volcanic activity therefore requires, as one component of risk, an estimation of the hazard posed by these phenomena (Brown et al., 2015; Magill and Blong, 2005a; Pareschi, 2000). Hazard estimates that are quantitative and probabilistic are preferred for the purposes of decision support tools (Marzocchi and Woo, 2007; Sandri et al., 2012), measuring or ranking risks (Magill and Blong, 2005a, 2005b), and as an objective measure for asset or land-use planning (Marzocchi et al., 2012). However, the specific impact of each process can range from minimal to catastrophic depending on eruption magnitude, style, intensity, and environmental interactions with the landscape and atmosphere (Hill et al., 2009). The large input space created by these eruption properties that can span several orders of magnitude, and many potential states of eruption style and environmental conditions form a critical obstacle to quantitative hazard assessment (Stirling et al., 2017; Stirling and Wilson, 2002).

Here we refer to quantitative hazard assessments as those that provide a probabilistic estimate of hazard intensity for one or many volcanic phenomena (Connor et al., 2015; Marzocchi et al., 2012) and hazard intensity as the magnitude of a hazard metric such as height, velocity or pressure (Wilson et al., 2012). In the framework of probabilistic volcanic hazard assessment (PVHA, Stirling et al., 2017; Stirling and Wilson, 2002), quantification at any site of interest consists of four broad steps: (1) identification of volcanic sources that may generate hazardous phenomena; (2) estimation of magnitude-frequency relationship for the eruption source; (3) quantifying the dependence of hazard intensity on the eruption magnitude, site properties and environmental conditions; and (4) estimation of hazard exceedance from the magnitude-frequency and hazard intensity relationships. This follows a similar methodology to probabilistic seismic hazard assessments (PSHA), exploiting the relatively early development (Cornell, 1968) and acceptance of seismic

* Corresponding author.
E-mail address: s.mead@massey.ac.nz (S.R. Mead).

https://doi.org/10.1016/j.cageo.2023.105417
Received 15 December 2021; Received in revised form 15 July 2023; Accepted 17 July 2023
Available online 23 July 2023

hazard modelling (Hill et al., 2009; Stirling et al., 2017).

The most mathematically complex elements in the PVHA approach occur in steps 2 and 3 (Stirling et al., 2017), which do not have accepted or easily computable solutions. Regarding the eruption source model in step 2, data completeness uncertainties (Coles and Sparks, 2006; Deligne et al., 2010; Wang and Bebbington, 2012) and intervolcano variation (Bebbington, 2014) affect frequency-magnitude relationships. These are further complicated by the range of eruption durations, style and transitions between styles (Bebbington and Jenkins, 2019) that may affect hazard intensity. Baseline probabilities of when and how large an eruption may be estimated through data (Damaschke et al., 2018; De La Cruz-Reyna, 1996; Decker, 1986; Klein, 1982; Marzocchi and Zaccarelli, 2006; Mendoza-Rosas and De la Cruz-Reyna, 2008; Mulargia et al., 1987) or expert elicitation approaches (Aspinall et al., 2003, 2006; Bebbington et al., 2018), and can be used to calculate conditional probabilities through event trees (Marzocchi et al., 2008; Newhall and Hoblitt, 2002) for hazard occurrence, eruption intensity, size and style. Provided with an eruption source model, the most logical approach to calculate hazard exceedance is through cross-multiplication of the source probability distributions with a hazard intensity model (e.g., Bevilacqua et al., 2017).

Numerical or statistical models that simulate volcanic processes (e.g., through commonly used simulation packages Titan2D, VolcFlow, Fall3D, Tephra2) are most often used to quantify hazard intensity as they also consider the effect of relevant site properties such as terrain between source and site and environmental conditions such as wind speed and direction for ash fall. Hazard assessments using this PVHA approach have mainly been applied to ashfall hazard with either a single source (Biass et al., 2016; Bonadonna et al., 2005; Hurst and Smith, 2004) or a multi-source region (Hurst and Smith, 2010; Jenkins et al., 2012; Magill and Blong, 2005a), using Monte Carlo methods to sample the input space for simulation parameters. This is often possible through limiting input variables to only a few dimensions. The dominance of probabilistic ashfall hazard assessments (Calder et al., 2015) is mainly due to the availability of simulators that are fast enough to be directly used in Monte Carlo analyses. However, when applied to more computationally expensive simulators such as the Titan2D suite for volcanic mass flows (Patra et al., 2005), Monte Carlo methods become infeasible (Mahmood et al., 2015). Critically for volcanic hazards, input distributions may change throughout a volcano's lifecycle, episode or eruption event (see Jenkins et al., 2007 for terminology). This may require updating and further simulations of the processes (Spiller et al., 2014).

Monte Carlo approaches that sample simulator inputs differ from PSHA, and the Stirling et al. (2017); Stirling and Wilson (2002) conceptual outlines of PVHA, where a functional approximation of hazard intensity is used. These functions are often linear transformations, producing a hazard surface that can be rapidly queried to estimate hazard intensity, and its uncertainty for the entire spectrum of untested inputs. A classic example of such mappings are ground motion prediction equations in seismology, but similar mappings (Bebbington et al., 2008; Rhoades et al., 2002) have been developed for ashfall based on the geologic record. A critical obstacle is developing functional approximations for pyroclastic flows, lahars and debris avalanches where robust models are difficult to develop from the geologic record due to physical processes such as erosion that mask smaller events in the record and large variability in flow initiation and dynamics. A proposed solution to this problem (Bayarri et al., 2009; Rutarindwa et al., 2019; Spiller et al., 2014) is to use an emulator, a fast statistical surrogate to computationally expensive simulations (Kennedy and O'Hagan, 2001; Rasmussen and Williams, 2006; Sacks et al., 1989). In simple mathematical notation, where a simulator produces outputs y as a function of the input configuration x as $y = f(x)$, an emulator is a suitably fast and accurate approximation of $f(x)$ that can be substituted to find y at unsimulated inputs.

In this study, we focus on the use of emulation as a functional approximation for step 3 of PVHA to create a probabilistic hazard assessment of dome collapse volcanic mass flows. Emulation techniques have been applied to volcanic mass flow hazards (e.g., Bayarri et al., 2009; Dalbey et al., 2008; Gu et al., 2018; Mahmood et al., 2015; Rutarindwa et al., 2019; Spiller et al., 2014; Stefanescu et al., 2012a), but focus on emulation to identify a specific catastrophic threshold at a point (Bayarri et al., 2009; Spiller et al., 2014) or across a spatial area (Dalbey et al., 2008; Rutarindwa et al., 2019; Stefanescu et al., 2012a). The use of specific thresholds of hazard intensity is largely incompatible with multi-hazard assessments that require the range of hazard sources and intensities at a specific location (Carpignano et al., 2009; Nadejda et al., 2016). Our method uses warped Gaussian processes (Snelson et al., 2004) to simplify elements of the previous approaches that require sub-emulators (Rutarindwa et al., 2019; Spiller et al., 2014) and provide a continuous estimate of hazard intensity that can be used to estimate exceedance. Using a location-centred approach, we refine and develop a PVHA methodology for volcanic mass flows to provide probabilistic hazard forecasts that integrate statistical modelling of source parameters, emulation methods and numerical simulations. This is demonstrated in an application to (probabilistically) forecast dome collapse flow height from Taranaki Volcano, New Zealand.

2. Methods used in probabilistic hazard assessment

2.1. Overview

A conceptual overview of the probabilistic hazard assessment process is shown in Fig. 1. At the location of interest, the individual hazard exceedance probability is determined through models of the hazard intensity ('Intensity-magnitude model' in Fig. 1) and its dependence on magnitude, site properties and environmental conditions and the hazard source (i.e. the occurrence probability of magnitude, properties and environmental conditions, 'Hazard source model' in Fig. 1). The source model produces values in the input space according to their probability distribution, which are then used to sample the hazard intensity model and define the exceedance function. Hazard source models for mass flows require the definition of a frequency-volume relationship, which is often conditional on probabilities of an eruption and specific eruptive phases, in addition to relationships for site properties such as flow direction (Wolpert et al., 2018).

The source model probability spaces are mostly real-valued and likely to change in response to volcanic activity, therefore a continuous and easily sampled intensity model is preferred. However, the common approach of using discrete simulations to identify hazard intensity (Bonadonna et al., 2005; Gallant et al., 2018; Mead and Magill, 2017; Patra et al., 2020) is computationally expensive and cannot account for changes in the distribution of the source model without re-simulation (Rutarindwa et al., 2019). This limitation is alleviated through use of a statistical surrogate in the form of a Gaussian process emulator to model mass flow hazard intensity as a continuous function. A general framework for surrogate modelling using Gaussian process emulation is reasonably well established from earlier literature (Bayarri et al., 2009; Kennedy and O'Hagan, 2001; Spiller et al., 2014). First, the hazard intensity at a set of predefined points within the input space is calculated using a computationally expensive, deterministic simulator ('Hazard simulations', Fig. 1), with sample points chosen using a space filling design (Santner et al., 2003). Then, the simulation inputs and outputs are used as training data for the emulator to create a computationally efficient, continuous approximation of the simulator ('Intensity-magnitude model', Fig. 1).

We use previously established source models and methods in this probabilistic hazard assessment, and therefore focus our methodology description on the simulation and emulation components of the surrogate modelling procedure to produce a hazard intensity model.

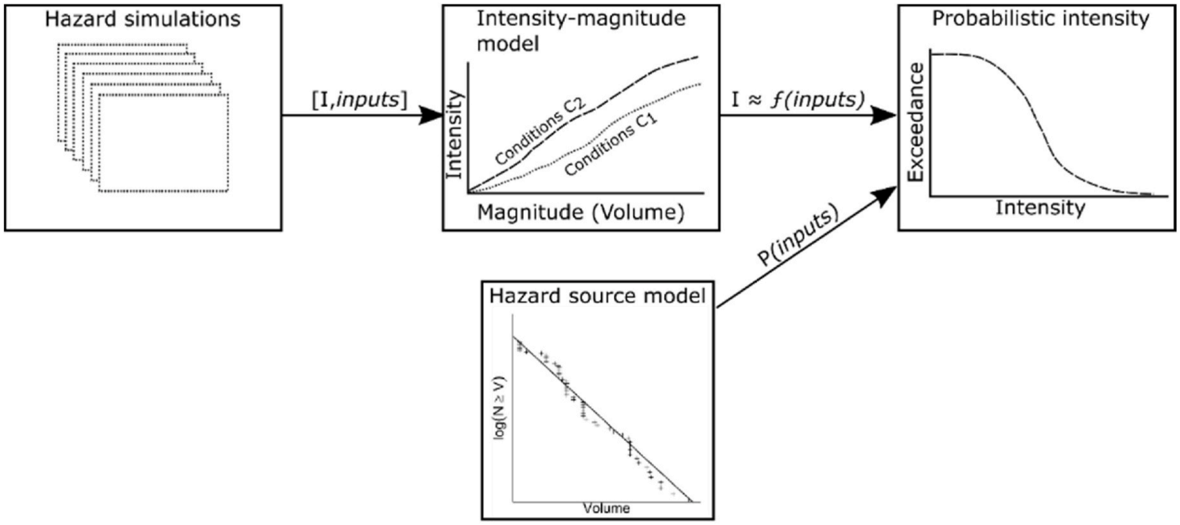

Fig. 1. The probabilistic mass flow hazard assessment process.

2.2. Volcanic mass flow simulation

Volcanic mass flows include dilute mixtures of particles in air (e.g. pyroclastic surges), dense, granular dominated flows (e.g., pyroclastic flows, block-and-ash flows) and, mixtures of granular material and water (lahars, debris avalanches, debris flows). The depth of these flows are typically much smaller than their large spatial extent. Depth-averaged simulation approaches which reduce computational complexity through a shallow-layer approximation are therefore well suited and frequently applied to the prediction of volcanic mass flow hazards (e.g., Aguilera et al., 2004; Bayarri et al., 2009; Charbonnier and Gertisser, 2009; Kelfoun et al., 2017; Mead and Magill, 2017; Patra et al., 2005; Pitman et al., 2003; Procter et al., 2010). The depth averaged system of equations in Cartesian coordinates can be expressed in terms of the height and momentum vector **U**, directional (x, y) flux vectors **F**, **G** and source (driving forces) vector **S** as:

$$\frac{\partial \mathbf{U}}{\partial t}+\frac{\partial \mathbf{F}}{\partial x}+\frac{\partial \mathbf{G}}{\partial y}=\mathbf{S} \tag{1}$$

We use a Mohr-Coulomb rheological model (Pitman et al., 2003) implemented in the Titan2D platform (Patra et al., 2005; Sheridan et al., 2005) for this application. The Mohr-Coulomb model for granular mass flows requires the following user specified inputs:

1. The terrain,
2. The initial volume, and its spatial distribution,
3. An internal friction angle φ, and
4. A basal friction angle, φ.

The same internal friction angle is used for all simulations in this study as previous studies have shown simulation results to be relatively insensitive to internal friction angles between 25° and 35° (Procter et al., 2010; Sheridan et al., 2005). The same terrain input is also used for all simulations. Terrain is commonly regarded as a fixed input for simplicity, however is often subject to considerable uncertainty (Hawker et al., 2018; Stefanescu et al., 2012a), and may change throughout a volcanic crisis. The basal friction angle characterises the mobility of volcanic flows, expressed as $\tan(\varphi)$, and is related to the flow volume (Pudasaini and Miller, 2013). With the terrain and internal friction angles fixed and basal friction angle having a fixed relationship with volume, the input space of the simulator (χ) therefore consists of the variables needed to define the initial pyroclastic flow volume and its location. These inputs can be most conveniently and efficiently parameterised as an ellipsoid with constant aspect ratios (e.g. Procter et al., 2010) requiring the definition of four inputs: an initial volume (v), location (North and East coordinates; N, E) and orientation (azimuth, θ) of the elliptical pile.

While the application described here uses and makes simplifications on the basis of the Mohr-Coulomb depth-averaged approximation in Titan2D, the emulation procedure (described in following section) treats the simulator as a 'black box' consisting only of inputs and outputs. As a result, our framework is not restricted to the simplifications specifically mentioned here. Alternative simulators and rheological models for depth averaged systems of equations (e.g., Iverson and George, 2014; Kelfoun, 2017; Pudasaini, 2012) may be substituted and additional inputs may be added with few methodological differences to the emulator.

2.2.1. Surrogate modelling of mass flow simulations

The simulator will produce a set of outputs, such as flow depth and dynamic pressure, for each simulation grid cell at any combination of the 4-dimensional input space ($\chi = [v, N, E, \theta]$), but at a great computational expense (~12–24 h on a 12-core processor). Our goal is to develop an emulator, a fast and computationally cheap surrogate for the simulator that provides an efficiently sampled functional representation of the input space. The emulation approach applied here borrows from the Bayarri et al. (2009); Gu et al. (2018); Spiller et al. (2014) Gaussian Process (GP) emulator methodology. The reader is referred to these publications for the full mathematical details, here we summarise the practical elements and key variations from the previous approaches important to this study.

Representing a scalar output of interest (y) from the simulator as $y = f(\mathrm{x}); (\mathrm{x} = [v, N, E, \theta])$, the GP emulator is a substitute for $f(\mathrm{x})$ as follows:

$$f(\mathrm{x}) \sim GP(\mu(\mathrm{x}), k(\mathrm{x}, \mathrm{x}')) \tag{2}$$

$$y \sim GP(\mu(\mathrm{x}), k(\mathrm{x}, \mathrm{x}'))\# \tag{3}$$

Where $\mu(\mathrm{x})$ is the mean (trend) with respect to x, and $k(\mathrm{x}, \mathrm{x}')$ is the covariance function across input pairs. The mean function $\mu(\mathrm{x})$ is often taken as zero or a fixed basis expansion for simplicity, as it simply normalises (to $\mu(\mathrm{x})$) the differences in x (Rasmussen and Williams, 2006).

The covariance function or kernel (Lloyd et al., 2014; Rasmussen and Williams, 2006) defines the correlation structure between inputs (x, x') across the input dimensions, controlled by a set of free parameters called hyperparameters. A useful feature of kernels is that they can be combined across and within input dimensions as a sum or product of different kernels (e.g. $k(\mathrm{x}, \mathrm{x}') = k_1(\mathrm{x}, \mathrm{x}') + k_2(\mathrm{x}, \mathrm{x}')$). This compositional property is convenient for model selection and aids interpretability (Duvenaud et al., 2013), as covariance functions can be defined for each dimension individually (a conceptually simple task for domain experts) rather than *en masse*. For computer simulation outputs, smoothing kernels such as the squared exponential and Matérn kernels are most commonly used (e.g., Bayarri et al., 2009; Gu et al., 2018; Rutarindwa et al., 2019; Spiller et al., 2014). The lengthscale, ℓ, is the free parameter in these smoothing functions indicating the correlation distance between input values, small lengthscales indicate a strong correlation in outputs between nearby input values whereas very long lengthscales indicates the correlation is almost independent of the input value.

In our simulations, expecting some degree of multi-scale variation as the pile volume and location changes, we choose a Matérn 3/2 kernel for the volume, North and East dimensions. In the orientation dimension, we expect smoother correlation and choose a periodic Matérn 5/2 kernel, with a period of π due to symmetry of the ellipse. Our covariance kernel is therefore:

$$k(\mathrm{x_i}, \mathrm{x_j}) = \prod k_{x=[v,N,E,\theta]}(\mathrm{x_i}, \mathrm{x_j}) \tag{4}$$

where

$$k_{x=[v,N,E]}(\mathrm{x_i}, \mathrm{x_j}) = \left(1 + \frac{\sqrt{3}r}{\ell}\right)\exp\left(-\sqrt{3}r\big/_{\ell}\right), \mathrm{x} = [v, N, E] \tag{5}$$

$$k_{x=\theta}(\mathrm{x_i}, \mathrm{x_j}) = \left(1 + \frac{\sqrt{5}r}{\ell} + \frac{5r^2}{3\ell^2}\right)\exp\left(-\sqrt{5}r\big/_{\ell}\right), \mathrm{x} = \theta \tag{6}$$

$$r = |\mathrm{x}_i - \mathrm{x}_j| \tag{7}$$

with ℓ being the lengthscale, and r the distance between the *ith* and *jth* input.

Inserting equations (4)–(6) into equation (3) defines a function parameterised with 4 unknown lengthscales of $k_{v,N,E,\theta}$ and the mean function. Estimating the lengthscale hyperparameters using Maximum Likelihood Estimation (MLE) is often unstable (Gu et al., 2018; Spiller et al., 2014). This issue can be solved through specification of a prior (the 'reference prior', Berger et al., 2001) and using the maximum a posteriori estimate (Bayarri et al., 2009; Spiller et al., 2014). We use the jointly robust prior of Gu (2019), an easily computable objective prior with similar properties to the reference prior (Berger et al., 2001) that yields a proper posterior distribution.

Another difficulty encountered in GP emulation of mass flow simulations is the presence of zero values in flow height, the quantity of interest. At any location a reasonable distance from the source, a large portion of the simulation input space of volume, ellipse location and orientation will produce an output value of zero, abruptly changing to non-zero and then increasing monotonically with volume. Such an output is non-stationary, a property which causes difficulty when fitting the GP emulator (Spiller et al., 2014). Solutions to this problem have been proposed and include partitioning (Gramacy and Lee, 2008), input or output warping (Snelson et al., 2004; Snoek et al., 2014) and non-stationary covariance functions (Paciorek and Schervish, 2004). For this task we found warping of the model output vector produced the most robust results. This approach, outlined in Snelson et al. (2004), transforms the model outputs ($\mathrm{y_m}$) by a series of hyperbolic tangent (*tanh*) steps with a linear trend outside the function bounds:

$$f(\mathrm{y_m}; \{a, b, c\}) = \mathrm{y_m} + \sum_{i=1}^{I} a_i \tanh(b_i(\mathrm{y_m} + c_i)) \quad a_i, b_i \geq 0 \tag{8}$$

Where a scales the step size, b the steepness and c controlling step position for any number of I steps. We use a single step in this study as our output data has a single step, although any number of steps could be used.

Following Gu and Berger (2016), we add a noise term in equation (3) to approximate $y = f(x) + \varepsilon$), as the basal friction input is masked from the emulator. The final emulator therefore contains 8 parameters (3 from equation (8) and (4) lengthscales and the noise term, which was optimised using a SCG optimisation algorithm through the GPy package (GPy, 2012).

3. Emulation of dome collapse flows at Mt. Taranaki

3.1. Geologic setting and eruptive history of Mt. Taranaki, New Zealand

Mt. Taranaki (2518 m) is near-symmetrical andesitic stratovolcano with more than 170,000 years of geologic history (Alloway et al., 2005). The volcanic activity of Mt. Taranaki is cyclical, with large, unconfined debris avalanches initiated by destruction of former Taranaki edifices beginning the cycle (Zernack and Procter, 2021). Regrowth of the Taranaki cone follows through smaller-scale activity, including small explosive eruptions, lava flows and dome growth. This activity can shift into larger scale explosive activity with large Plinian and sub-Plinian eruptions; block-and-ash flows; and the generation of long-runout, but confined mass flows (Zernack and Procter, 2021).

Activity since the last debris avalanche ~7000 years ago is represented through a regrowth phase of 53 different eruption episodes identified in proximal deposits on Taranaki (Torres-Orozco et al., 2017b). These indicate complex eruption sequences associated with the generation of ashfall deposits and small-scale pyroclastic density currents from eruption columns, longer-runout block-and-ash flows, and syn-eruptive or secondary lahars following valley and river channels in the Taranaki region (Torres-Orozco et al., 2017b). The most recent period of activity, the Maero Eruptive Period, began approximately 1000 years ago (Lerner et al., 2019; Neall, 1979; Platz et al., 2007) and is characterised by small eruptions (Volcanic Explosivity Index 3–4) with emplacement and collapse of lavas and smaller domes on the summit of Mt. Taranaki (Lerner et al., 2019; Neall et al., 1986; Torres-Orozco et al., 2017a; Zernack et al., 2009). It is uncertain if the Maero Eruptive Period has terminated, and the next eruption of Taranaki is therefore expected to have similar eruption characteristics and summit vent location to those in the Maero Eruptive Period (Lerner et al., 2019).

A detailed account of pyroclastic flows during the Maero Eruptive Period is reported in Platz et al. (2007) who identified at least 10 separate flow events over the past 900 years. These flows affected two main sectors of Mt. Taranaki: the W-NW sector towards Stony (Hangatahua) River and the N-NE sector towards Ahukawakawa Swamp (Fig. 2). This distribution of dome collapse pyroclastic flows is strongly influenced by the summit morphology (Lerner et al., 2019). Currently, the summit contains remnants of a lava dome (~1.5×10^6 m^3) within a 420 m diameter crater breached from the SW to NE towards the Stony River, called 'The Chute' (Platz et al., 2007). This morphology directs most block-and-ash flows towards the NW sector of Egmont National Park; the past ~800 years of block-and-ash flows have almost exclusively impacted this sector (Procter et al., 2010). The hazard is assessed across three different locations (shown in Fig. 2) to compare and quantitatively examine the effect of this morphology.

3.2. Simulation of dome collapse pyroclastic flows

Dome collapse flows from the Taranaki summit appear to have lower energy in contrast to lateral blast triggered pyroclastic density currents, and dynamics are approximated well with a Mohr-Coulomb rheological model (Platz et al., 2007; Procter et al., 2021). Unit volumes for the Maero Eruptive Period dome collapse flows range from 1 to 15 $\times 10^6$ m^3, but likely represent a collection of smaller flows (Procter et al., 2010). A previous study of summit dome collapses (Procter et al., 2010) simulated flows with a volume of 10^6 m^3 using the Mohr-Coulomb model in Titan2D, which matched well to mapped deposits with similar volumes. Our simulation study introduces more variation to the summit dome configuration.

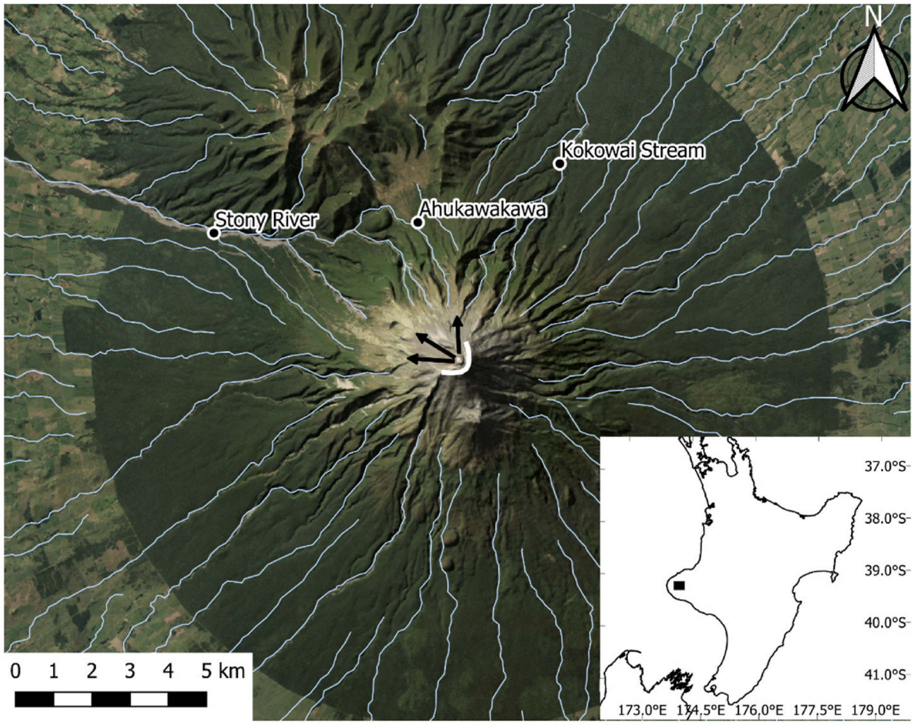

Fig. 2. Taranaki volcano in Egmont National park with flow measurement points used in this study. Inset map shows location of Taranaki Volcano within New Zealand North Island Arrows show major flow paths for block-and-ash flows during the Maero eruptive period (Platz, 2007), white line shows crater rim and blue lines indicate stream centrelines.

A half-ellipsoidal collapse shape was assumed with aspect ratios matching those of the previous dome (Platz, 2007) and volumes ranging from 10^5 to 10^7 m^3. The maximum volume corresponds to the presumed maximum dome volume possible in the summit crater, but is larger than the maximum dome collapse flow volumes expected at Taranaki (Procter et al., 2010). We specified a larger volume in this case to expand the simulation input space beyond expected volumes to ensure adequate support for the surrogate modelling and sampling, similar to Rutarindwa et al. (2019). Similar expanded input spaces were used to vary the planimetric centre and orientation of the dome, accounting for scenarios where a new dome is emplaced on the summit following an explosive eruption to clear the remnant dome (Ogburn et al., 2015). The centre of the collapsing ellipse from the summit vent was varied in polar coordinates (0–210 m radius, 0 to 2π angle), transformed into planimetric (N, E) coordinates for input. The orientation of the ellipse major axis was also varied between 0 and 180° (current orientation $\sim$117.5°). The internal friction coefficient, shown to have little effect on simulations (Procter et al., 2010; Sheridan et al., 2005), was set at 30° for all simulations. Basal friction was determined as a function of volume using the friction-volume relationship for volcanic mass flows (Pudasaini and Miller, 2013). A total of 1024 input configurations (a set of $[v, N, E, \theta]$) were simulated, with inputs chosen in a Latin hypercube space filling design. All simulations used a 1 m digital elevation model (DEM) derived from LiDAR surveys in October 2021. This DEM was downsampled to 10 m for computational efficiency. High resolution DEM's are generally preferred for accurate mass flow simulation (Capra et al., 2011; Stefanescu et al., 2012b; Stevens et al., 2003), however the 10 m DEM provides the best balance between computational efficiency and accuracy. While flow estimates in the simulations will likely be affected by the lack of representation of features smaller than 10 m horizontally, these effects have been shown to be less critical for accuracy if flow volume is greater than 10^5 m^3 (Stefanescu et al., 2012b), slopes are $<4°$ and topography has simple drainage paths (Stevens et al., 2003).

The simulation output of interest (y from Equation (3)) in this study is the maximum flow depth throughout the entire simulation. Results from all simulations are shown in Fig. 3, aggregated to show the minimum volume required to exceed a threshold flow height of 0.5 m, typical heights for a catastrophic flow are between 0.25 and 1.0 m (Spiller et al., 2014). The simulations show most valleys within Egmont National Park are affected by dome-collapse flows in the range of dome configurations described, and that maximum flow depth increases with volume in a largely monotonic manner. Across the three locations in this study, flows need to exceed a critical volume (5.0×10^6 for Stony River, 2.5×10^6 for Kokowai Stream and Ahukawakawa swamp) to cause flow height above the 0.5 m threshold. However, the simplistic assessment in Fig. 3 disregards the effect of location and orientation input variables. This can be explored through the use of Gaussian Process emulator fitted to data for the three locations in Fig. 2.

3.3. Emulator

Leave-one-out cross-validation (LOO-CV) is used to evaluate performance of the emulator as a predictor. In LOO-CV, the emulator is used to predict a single, left-out, simulator output using the remaining simulator outputs. This process is repeated for each output of the simulator. Fig. 4 shows leave-one-out cross-validation results calculated using Vehtari et al. (2016) for the emulators fitted to each location of interest. The emulator mean is within 2 standard deviations of almost all ($>$90%) of the simulated values, although the errors (red in Fig. 4) show some bias towards over-estimation at very low simulated height. Over-estimation is preferred to underestimation in terms of risk, and uncertainties at very low heights are expected to have less of an effect on estimated hazard.

The emulators can be used to examine 'slices' of the input space by providing a continuous estimation across any dimension or combination of dimensions. Two examples of these are shown in Figs. 5 and 6. Fig. 5 shows the emulator mean and 95% confidence interval for dome collapse flows with a location and orientation similar to the current dome and volume varying between 10^5 and 10^7 m^3. The prediction for Ahukawakawa (Fig. 5a) indicates flow heights are expected to be less

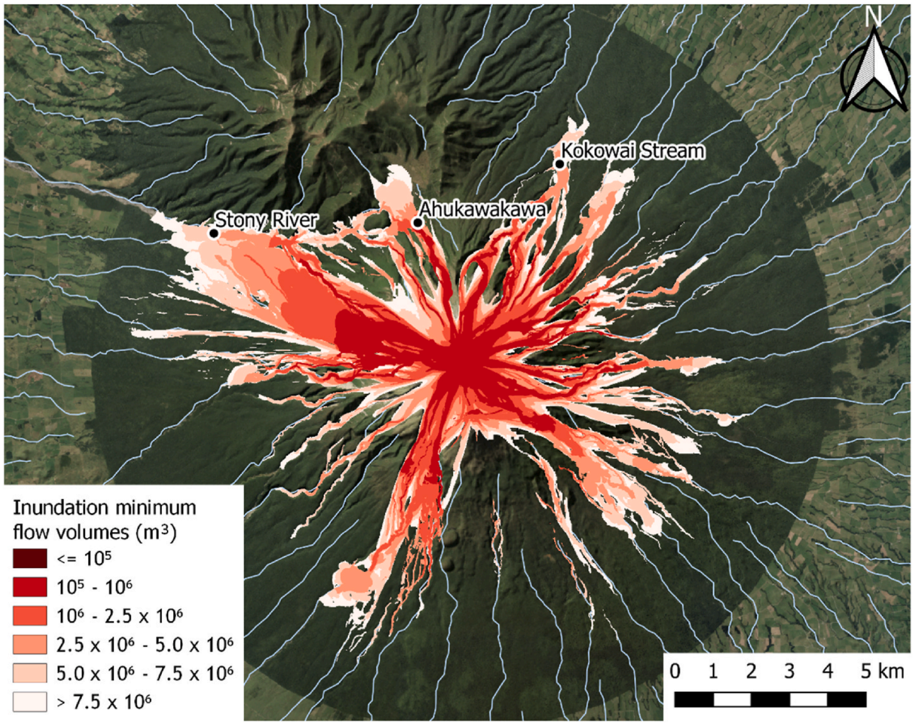

Fig. 3. Inundation limits of minimum block-and-ash flow volumes required to exceed 1.0 m in flow depth for all simulations.

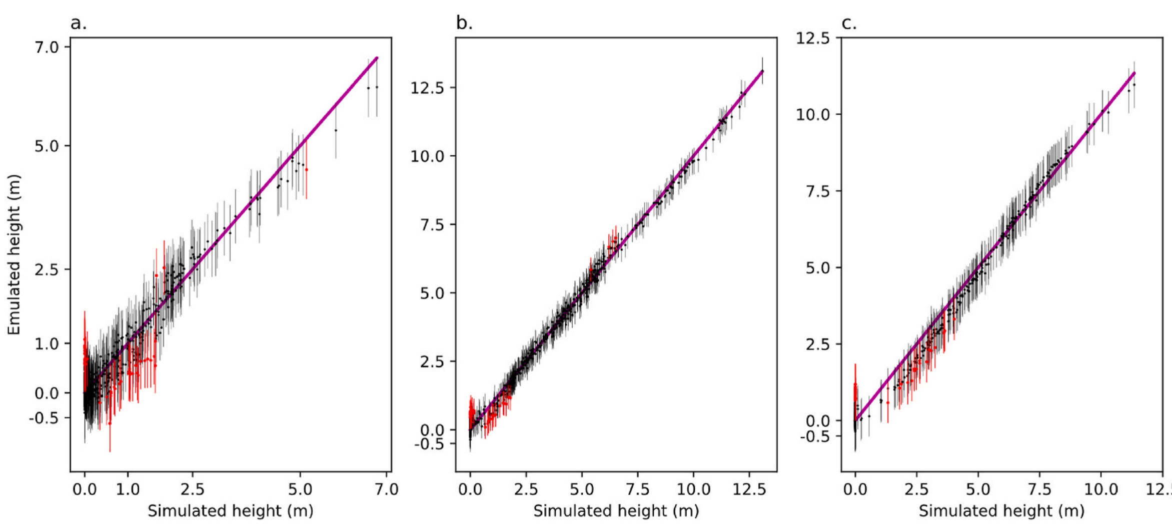

Fig. 4. Leave-one-out cross-validation results for emulators fitted to simulation data at (a) Ahukawakawa, (b) Stony River, and (c) Kokowai Stream. Dots indicate the mean estimate, error lines are ±2 standard deviations of the mean, red points highlight estimates that are greater than 2 standard deviations from the simulated flow height. Magenta line indicates a perfect fit.

than 2.5 m in any volume scenario with the current dome configuration. The emulated flow height is much higher for Stony River, in agreement with the observations of a preferential flow direction in Platz et al. (2007). Emulated heights for Kokowai Stream also indicate a critical volume ($>5.0 \times 10^6$ m^3) is necessary to overcome topographic barriers and direct flow towards this location.

Emulator slices can also be used to estimate the effect of new dome configurations following explosive modification of summit. For example, Fig. 6 shows an example of emulated flow heights for a dome collapse volume of 7.0×10^6 m^3 across the major axis orientation which can be used to evaluate directionality effects of dome collapse flows. A circular shape would indicate the dome major axis has no effect on maximum flow height and there are no directionality effects. Fig. 6 shows clear variations in flow height with major axis angle, with a preference for larger flow heights when the dome is oriented towards the stream location.

4. Application to dome collapse hazard assessment

Referring to Fig. 1, probabilistic hazard assessment requires both an easily sampled surrogate and a source model quantifying the probability of the input space. The exceedance probability of flow height can then be calculated using Monte Carlo samples of the source distributions to calculate flow height in the emulator (i.e. similar to Bebbington et al., 2008). With the emulator built, and uniform distributions assumed for the dome orientation and location (N, E, θ) due to a lack of prior

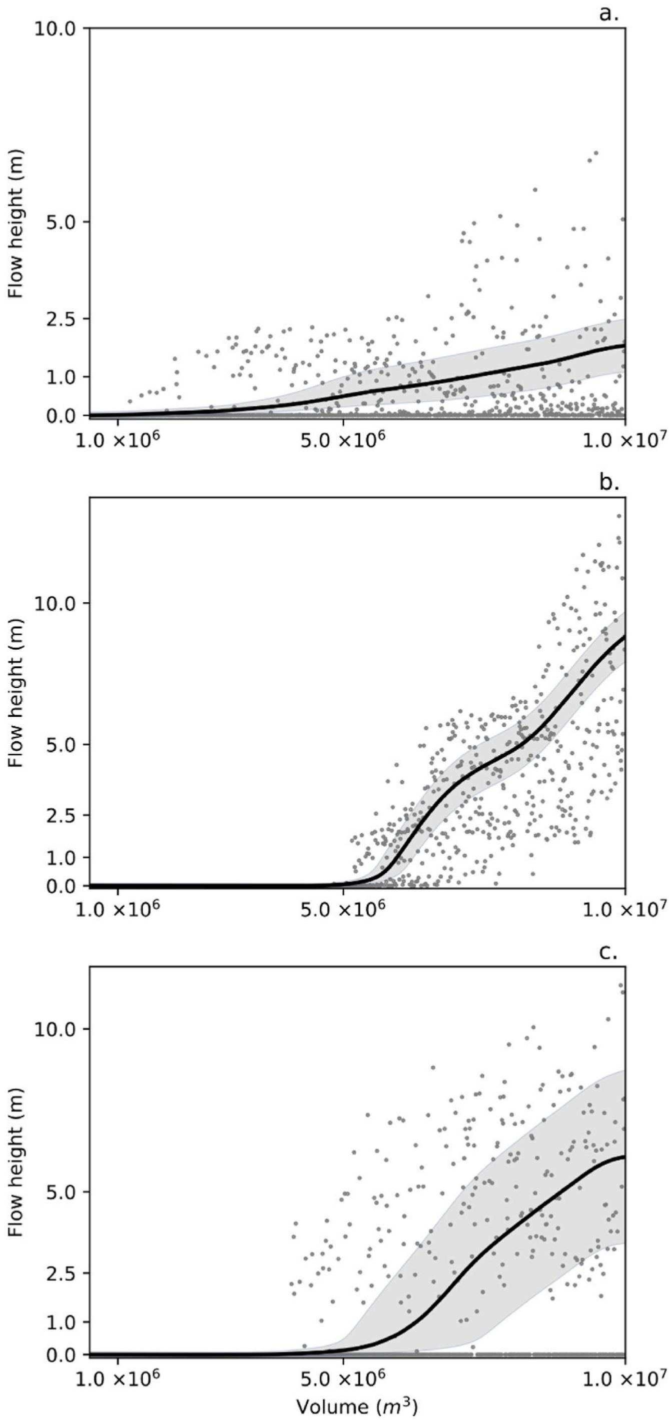

Fig. 5. Emulator mean (black line) and 95% confidence interval (shaded) predictions for dome collapse flows in a similar configuration to the current (remnant) Taranaki dome at (a) Ahukawakawa, (b) Stony River, and (c) Kokowai Stream locations. Grey dots indicate simulated flow heights from all simulations.

information, a frequency-volume distribution is required to define the hazard.

Fig. 5 suggests dome collapse volumes need to be greater than the current remnant dome volume (~1.5 × 10^6 m^3) to cause flow heights greater than 0.5 m. Dome collapses of this magnitude have occurred at Taranaki, the most recent summit dome volume was estimated to be ~5.9 × 10^6 m^3 in volume before collapse (Platz et al., 2012). However, an episode of significant dome growth is required to generate such

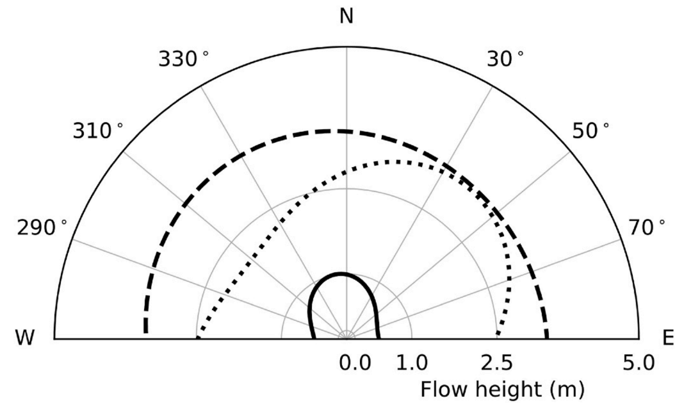

Fig. 6. Emulator mean predictions for dome collapse flow volumes of 7.0 × 10^6 m^3 with a similar configuration to the current (remnant) Taranaki dome and varied major axis orientation at Ahukawakawa (solid line), Stony River (dashed line), and Kokowai Stream (dotted line) locations.

conditions. Therefore, the likelihood of block-and-ash flows affecting the locations of interest is limited by the occurrence of a sufficient dome growth episode.

As there is no direct evidence of dome growth and collapse at Mt. Taranaki, we use the '*DomeHaz*' global dome growth dataset and analysis of Ogburn et al. (2015) to identify pathways to dome growth episodes capable of generating hazardous flows. The Ogburn et al. (2015) analysis notes it is most common to have an explosive eruption before dome growth episodes. They posit that large explosive eruptions may be necessary before dome growth episodes to remove high viscosity (i.e. cold) magma and lava from the conduit and enable extrusion of large magma volumes. This hypothesis is also supported by Platz (2007), using evidence from the Maero Eruptive Period. Assuming an explosive eruption is required to precede a new episode of dome growth capable of producing hazardous block-and-ash flows, and using the minimum dome extrusion rate (6.0 m^3s^{-1}) for the latest dome growth episode (Pyramid, Platz, 2007); the probability tree of Ogburn et al. (2015) suggests there is a 0.73 probability of a dome growth episode, if an eruption occurs. This probability (0.73) relates to the chance of a dome growth episode following an eruption. As most lava domes do not collapse completely (Ogburn and Calder, 2017; Platz et al., 2007), instead releasing 50%–80% of their total dome volume, the probability of dome collapse volumes, conditional on a sufficient growth episode needs to be calculated. A power-law distribution ($p(x) \propto x^{-\alpha}$) was used to fit andesitic dome collapse volumes in the Global Archive of Dome Instabilities database (Harnett et al., 2019). The frequency-volume plot in Fig. 7 shows the data are well-fit by the distribution between 1.5 × 10^6 and 10^7 m^3 with an α of 1.78. The exceedance probability of flow height can then be estimated by sampling the emulator with dome volumes drawn from the power-law distribution up to a maximum of 10^7 m^3, and uniform distributions for dome location (within 150 m North and South of current dome location) and orientation.

Fig. 8 shows dome collapse flow height exceedance probability, conditional on a new dome growth episode, for all locations calculated from 10,000 dome configurations and 10 draws of the emulator posterior. Smaller flows (heights <1.0 m) are more likely at the Kokowai (dotted line) and Ahukawakawa (solid line) locations,. however, larger flows (>5 m) are much more likely to occur in the Stony River. These differences in exceedances are potentially due to the varying proximity to dome, origin of streams and topographic controls. Low volume flows, which have a higher probability, are more likely to reach the Kokowai Stream and Ahukawakawa locations due to their proximity to the summit, provided dome configuration conditions that direct flows down these catchments are met. However, most mass flows are directed along the Stony River catchment due to topographic controls (Procter et al., 2010). The distance from summit means smaller volume flows are

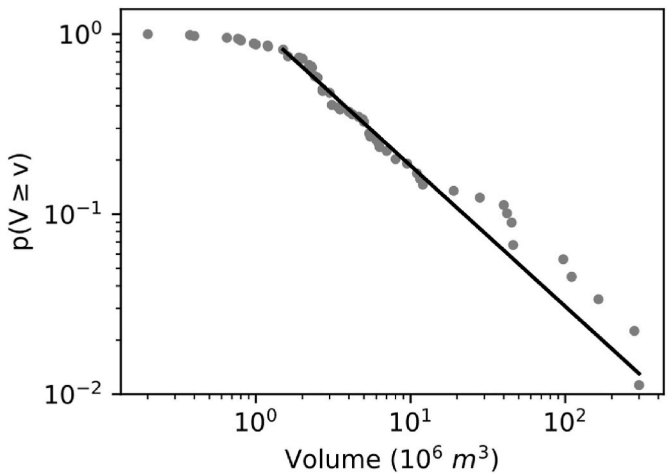

Fig. 7. Log-log scale plot of proportion of dome collapse flow volumes exceeding volume *V*. Dots are empirical data from Harnett et al. (2019), black line is best fit power-law (α ≈ 1.78) with a minimum volume of 1.5×10^6 m^3.

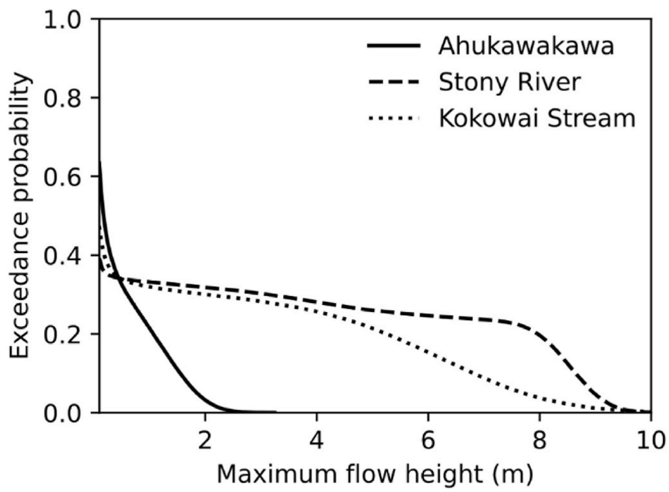

Fig. 8. Flow height exceedance probabilities for Ahukawakawa (black line), Stony River (dashed line), and Kokowai Stream (dotted line) locations. Probabilities are conditional on a new dome growth episode following an eruption (p = 0.73).

unlikely to reach the Stony River location. However, flows appear to have the same maximum height in this location once a critical volume is met (see Fig. 5b), resulting in an almost equal probability of exceeding flow heights between 2 and 4 m.

5. Discussion

The use of surrogate models to approximate hazard has several benefits for probabilistic hazard assessment over the estimates of hazard provided through simulations from numerical models. The emulators used here provide a continuous approximation of hazard across the entire input space of potential dome collapse flows, providing hazard assessments with flexibility to changing distributions of input parameters, support for analysis such as disaggregation, and alleviating the computational burden of numerical modelling.

The emulator supports easier updating of the hazard estimate in response to changes in source probabilities over numerical modelling. For example, the exceedance curves in Fig. 8 are derived from Monte-Carlo sampling of the emulator with the frequency-volume distribution shown in Fig. 7. These exceedance curves could be constructed through simulation, however any changes to the frequency-volume distribution would require a new set of simulations as opposed to simply resampling the emulator.

The functional approximation of hazard as a surrogate increases the ease of analysis through the ability to disaggregate results by different inputs to identify the relative effect of inputs on the hazard. This is demonstrated in Figs. 5 and 6, which are slices of the emulator response surface at fixed inputs of location and orientation (Fig. 5) or location and volume (Fig. 6). This can provide particular guidance into high-hazard outcomes, for example the preferential increase in flow height with dome orientation shown in Fig. 6.

The surrogate models proposed here provide a preferable solution to quantifying mass flow hazard in a probabilistic manner over brute force applications running many thousands of simulations, even if computational cost is not a factor for consideration. However, the surrogate emulators are particularly useful if the simulator has a high computational cost. The surrogate emulator can be rapidly sampled compared to a simulator, alleviating the computational burden when sampling using Monte-Carlo estimation. For example, the 300,000 (3 × 100,000) samples in this example (Fig. 8) took only 7 min on a desktop computer using an unoptimized sampling algorithm. In contrast, a single simulation using Titan2D can take up to 24 h in a high-performance, parallel computing environment.

These benefits can be limited by the simulation and simulator design space. If the simulation is inadequate or approximations are required outside the design space, the emulator will provide a bad fit to the process. These simulator inaccuracies may be addressed through informed model choice and calibration or model averaging (Akhavan-Safaei et al., 2017) as simulators are treated as a 'black box' by the emulator, only relying on the input (χ) and output (y) vectors. However, and uncertainties of the simulator will be propagated into limitations and uncertainties of the surrogate.

Definition of the input space can cause issues in emulation, as the space needs to be broad enough to cover all eventualities, while narrow enough to provide an adequate density of data for the emulator. In particular, non-stationarity is a difficult issue for mass flow emulation using Gaussian Processes (Rutarindwa et al., 2019; Spiller et al., 2014). Non-stationarity occurs in this data where the output changes from zero to positive flow height over a very small portion of input space, affecting Gaussian Process assumptions of constant mean and variance. Our approach to this problem used output warping (Snelson et al., 2004), which performed satisfactorily for this application (see cross-validation results in Fig. 4) and appears simpler to apply than previously suggested sub-emulators (Rutarindwa et al., 2019; Spiller et al., 2014).

6. Conclusion

This method of probabilistic hazard assessment using deterministic simulations via Gaussian Process emulators as a statistical surrogate for simulation results. The emulator created a linear mapping between dome collapse flow inputs (volume, location, orientation) and simulated maximum flow heights, with non-stationarity in outputs addressed using a warping function fit with the emulator. Emulators created at three locations for dome collapse flow simulations at Taranaki volcano, New Zealand were found to approximate the simulations well (>90% within 2 standard deviations using leave-one-out cross validation). These created emulators act as a fast engine for probabilistic volcanic hazard assessment, enabling the use of standard Monte Carlo methods to estimate dome collapse flow hazard. This method has been successfully applied to a probabilistic estimation of hazard at key locations within the Egmont National Park at Taranaki, the application of which will be explored in future work. This methodology incorporating deterministic simulations and gaussian process emulators is not specific to dome collapse flows, and can be readily applied to other volcanic hazards and geo-hazards in general, provided a well-defined input space.

Authorship contribution statement

SM wrote the code, performed simulations and hazard assessment, and drafted the manuscript. JP contributed to development of manuscript, hazard simulations, editing and revision of the manuscript. MB contributed to statistical modelling, editing and revision of the manuscript.

Computer code availability

The open-source python code for the Probabilistic Surrogate, including sample data, is available from https://github.com/stuartmead/probablisticsurrogate. Modified Titan2D simulator source code used to create the source data is available in the Zenodo repository https://doi.org/10.5281/zenodo.153993.

Declaration of competing interest

The authors declare that they have no known competing financial interests or personal relationships that could have appeared to influence the work reported in this paper.

Data availability

Data and code are provided in the Github repository. DEM data is publicly avaliable on the LiNZ data service.

Acknowledgements

The authors acknowledge the use of the New Zealand eScience Infrastructure (NeSI) high performance computing facilities as part of this research. Authors Mead and Bebbington were supported by the MBIE Endeavour Programme 'Transitioning Taranaki to a Volcanic Future' UOAX1913; Procter was supported by the Resilience to Natures Challenges Volcano programme GNS-RNC047. Digital Elevation data was sourced from the LINZ Data Service and licences by Taranaki Regional Council for re-use under the Creative Commons Attribution 4.0 International licence.

References

Aguilera, E., Pareschi, M.T., Rosi, M., Zanchetta, G., 2004. Risk from Lahars in the Northern valleys of cotopaxi volcano (Ecuador). Nat. Hazards 33, 161–189.
Akhavan-Safaei, A., Bevilacqua, A., Patra, A., Bursik, M., 2017. A Bayesian Framework for Rheology Model Combination and UQ in Simulation of Geophysical Mass Flows.
Alloway, B., McComb, P., Neall, V., Vucetich, C., Gibb, J., Sherburn, S., Stirling, M., 2005. Stratigraphy, age, and correlation of voluminous debris-avalanche events from an ancestral Egmont Volcano: implications for coastal plain construction and regional hazard assessment. J. Roy. Soc. N. Z. 35, 229–267.
Aspinall, W.P., Mader, H.M., Coles, S.G., Connor, C.B., Connor, L.J., 2006. Structured Elicitation of Expert Judgement for Probabilistic Hazard and Risk Assessment in Volcanic Eruptions, Statistics in Volcanology. Geological Society of London, p. 0.
Aspinall, W.P., Woo, G., Voight, B., Baxter, P.J., 2003. Evidence-based volcanology: application to eruption crises. J. Volcanol. Geoth. Res. 128, 273–285.
Bayarri, M.J., Berger, J.O., Calder, E.S., Dalbey, K., Lunagomez, S., Patra, A.K., Pitman, E.B., Spiller, E.T., Wolpert, R.L., 2009. Using statistical and computer models to quantify volcanic hazards. Technometrics 51, 402–413.
Bebbington, M., Cronin, S.J., Chapman, I., Turner, M.B., 2008. Quantifying volcanic ash fall hazard to electricity infrastructure. J. Volcanol. Geoth. Res. 177, 1055–1062.
Bebbington, M.S., 2014. Long-term forecasting of volcanic explosivity. Geophys. J. Int. 197, 1500–1515.
Bebbington, M.S., Jenkins, S.F., 2019. Intra-eruption forecasting. Bull. Volcanol. 81, 34.
Bebbington, M.S., Stirling, M.W., Cronin, S., Wang, T., Jolly, G., 2018. National-level long-term eruption forecasts by expert elicitation. Bull. Volcanol. 80, 56.
Berger, J.O., De Oliveira, V., Sansó, B., 2001. Objective bayesian analysis of spatially correlated data. J. Am. Stat. Assoc. 96, 1361–1374.
Bevilacqua, A., Neri, A., Bisson, M., Esposti Ongaro, T., Flandoli, F., Isaia, R., Rosi, M., Vitale, S., 2017. The effects of vent location, event scale, and time forecasts on pyroclastic density current hazard maps at campi flegrei caldera (Italy). Front. Earth Sci. 5.
Biass, S., Bonadonna, C., di Traglia, F., Pistolesi, M., Rosi, M., Lestuzzi, P., 2016. Probabilistic evaluation of the physical impact of future tephra fallout events for the Island of Vulcano, Italy. Bull. Volcanol. 78, 37.
Bonadonna, C., Connor, C.B., Houghton, B.F., Connor, L., Byrne, M., Laing, A., Hincks, T. K., 2005. Probabilistic modeling of tephra dispersal: hazard assessment of a multiphase rhyolitic eruption at Tarawera, New Zealand. J. Geophys. Res. Solid Earth 110 (n/a-n/a).
Brown, S.K., Jenkins, S.F., Sparks, R.S.J., Odbert, H., Auker, M.R., 2017. Volcanic fatalities database: analysis of volcanic threat with distance and victim classification. J. Appl. Volcanol. 6, 15.
Brown, S.K., Loughlin, S.C., Sparks, R.S.J., Vye-Brown, C., Barclay, J., Calder, E., Cottrell, E., Jolly, G., Komorowski, J.C., Mandeville, C., Newhall, C.G., Palma, J.L., Potter, S., Valentine, G., 2015. Global volcanic hazard and risk. In: Vye-Brown, C., Brown, S.K., Sparks, S., Loughlin, S.C., Jenkins, S.F. (Eds.), Global Volcanic Hazards and Risk. Cambridge University Press, Cambridge, pp. 81–172.
Calder, E., Wagner, K., Ogburn, S.E., 2015. Volcanic hazard maps. In: Loughlin, S.C., Sparks, R.S.J., Brown, S.K., Jenkins, S.F., Vye-Brown, C. (Eds.), Global Volcanic Hazards and Risk. Cambridge University Press.
Capra, L., Manea, V.C., Manea, M., Norini, G., 2011. The importance of digital elevation model resolution on granular flow simulations: a test case for Colima volcano using TITAN2D computational routine. Nat. Hazards 59, 665–680.
Carpignano, A., Golia, E., Di Mauro, C., Bouchon, S., Nordvik, J.P., 2009. A methodological approach for the definition of multi-risk maps at regional level: first application. J. Risk Res. 12, 513–534.
Charbonnier, S., Gertisser, R., 2009. Numerical simulations of block-and-ash flows using the Titan2D flow model: examples from the 2006 eruption of Merapi Volcano, Java, Indonesia. Bull. Volcanol. 71, 953–959.
Coles, S., Sparks, R., 2006. Extreme value methods for modelling historical series of large volcanic magnitudes. In: Mader, H., Coles, S., Connor, C., Connor, L. (Eds.), Statistics in Volcanology. Geological Society of London, pp. 47–56.
Connor, C., Bebbington, M., Marzocchi, W., 2015. Probabilistic volcanic hazard assessment. In: Sigurdsson, H. (Ed.), The Encyclopedia of Volcanoes, second ed. Academic Press, Amsterdam, pp. 897–910.
Cornell, C.A., 1968. Engineering seismic risk analysis. Bull. Seismol. Soc. Am. 58, 1583–1606.
Dalbey, K., Patra, A.K., Pitman, E.B., Bursik, M.I., Sheridan, M.F., 2008. Input uncertainty propagation methods and hazard mapping of geophysical mass flows. J. Geophys. Res. Solid Earth 113 (n/a-n/a).
Damaschke, M., Cronin, S.J., Bebbington, M.S., 2018. A volcanic event forecasting model for multiple tephra records, demonstrated on Mt. Taranaki, New Zealand. Bull. Volcanol. 80, 9.
De La Cruz-Reyna, S., 1996. Long-term probabilistic analysis of future explosive eruptions. In: Scarpa, R., Tilling, R.I. (Eds.), Monitoring and Mitigation of Volcano Hazards. Springer Berlin Heidelberg, Berlin, Heidelberg, pp. 599–629.
Decker, R.W., 1986. Forecasting volcanic eruptions. Annu. Rev. Earth Planet Sci. 14, 267–291.
Deligne, N.I., Coles, S.G., Sparks, R.S.J., 2010. Recurrence rates of large explosive volcanic eruptions. J. Geophys. Res. Solid Earth 115, B06203.
Duvenaud, D., Lloyd, J.R., Grosse, R., Tenenbaum, J.B., Ghahramani, Z., 2013. Structure discovery in nonparametric regression through compositional kernel search. In: Proceedings of the 30th International Conference on International Conference on Machine Learning, vol. 28. JMLR. org. III-1166.
Gallant, E., Richardson, J., Connor, C., Wetmore, P., Connor, L., 2018. A new approach to probabilistic lava flow hazard assessments, applied to the Idaho National Laboratory, Eastern Snake River Plain, Idaho, USA. Geology 46, 895–898.
GPy, 2012. A Gaussian process framework in Python. https://github.com/SheffieldML/GPy.
Gramacy, R.B., Lee, H.K.H., 2008. Bayesian treed Gaussian process models with an application to computer modeling. J. Am. Stat. Assoc. 103, 1119–1130.
Gu, M., 2019. Jointly robust prior for Gaussian stochastic process in emulation, calibration and variable selection. Bayesian Anal 14, 857–885.
Gu, M., Berger, J.O., 2016. Parallel partial Gaussian process emulation for computer models with massive output. Ann. Appl. Stat. 10, 1317–1347.
Gu, M., Wang, X., Berger, J.O., 2018. Robust Gaussian stochastic process emulation. Ann. Stat. 46, 3038–3066.
Harnett, C.E., Thomas, M.E., Calder, E.S., Ebmeier, S.K., Telford, A., Murphy, W., Neuberg, J., 2019. Presentation and analysis of a worldwide database for lava dome collapse events: the Global Archive of Dome Instabilities (GLADIS). Bull. Volcanol. 81, 1–17.
Hawker, L., Rougier, J., Neal, J., Bates, P., Archer, L., Yamazaki, D., 2018. Implications of simulating global digital elevation models for flood inundation studies. Water Resour. Res. 54, 7910–7928.
Hill, B.E., Aspinall, W.P., Connor, C.B., Godoy, A.R., Komorowski, J.C., Nakada, S., 2009. Recommendations for assessing volcanic hazards at sites of nuclear installations. In: Connor, C.B., Connor, L.J., Chapman, N.A. (Eds.), Volcanic and Tectonic Hazard Assessment for Nuclear Facilities. Cambridge University Press, Cambridge, pp. 566–592.
Hurst, T., Smith, W., 2004. A Monte Carlo methodology for modelling ashfall hazards. J. Volcanol. Geoth. Res. 138, 393–403.
Hurst, T., Smith, W., 2010. Volcanic ashfall in New Zealand – probabilistic hazard modelling for multiple sources. N. Z. J. Geol. Geophys. 53, 1–14.
Iverson, R.M., George, D.L., 2014. A depth-averaged debris-flow model that includes the effects of evolving dilatancy. I. Physical basis.
Jenkins, S., Magill, C., McAneney, J., Blong, R., 2012. Regional ash fall hazard I: a probabilistic assessment methodology. Bull. Volcanol. 74, 1699–1712.
Jenkins, S.F., Magill, C.R., McAneney, K.J., 2007. Multi-stage volcanic events: a statistical investigation. J. Volcanol. Geoth. Res. 161, 275–288.

Kelfoun, K., 2017. A two-layer depth-averaged model for both the dilute and the concentrated parts of pyroclastic currents. J. Geophys. Res. Solid Earth 122, 4293–4311.

Kelfoun, K., Gueugneau, V., Komorowski, J.-C., Aisyah, N., Cholik, N., Merciecca, C., 2017. Simulation of block-and-ash flows and ash-cloud surges of the 2010 eruption of Merapi volcano with a two-layer model. J. Geophys. Res. Solid Earth 122, 4277–4292.

Kennedy, M.C., O'Hagan, A., 2001. Bayesian calibration of computer models. J. Roy. Stat. Soc. B 63, 425–464.

Klein, F.W., 1982. Patterns of historical eruptions at Hawaiian volcanoes. J. Volcanol. Geoth. Res. 12, 1–35.

Lerner, G.A., Cronin, S.J., Bebbington, M.S., Platz, T., 2019. The characteristics of a multi-episode volcanic regime: the post-AD 960 Maero Eruptive Period of Mt. Taranaki (New Zealand). Bull. Volcanol. 81, 61.

Lloyd, J.R., Duvenaud, D., Grosse, R., Tenenbaum, J., Ghahramani, Z., 2014. Automatic Construction and Natural-Language Description of Nonparametric Regression Models.

Magill, C., Blong, R., 2005a. Volcanic risk ranking for Auckland, New Zealand. I: methodology and hazard investigation. Bull. Volcanol. 67, 331–339.

Magill, C., Blong, R., 2005b. Volcanic risk ranking for Auckland, New Zealand. II: hazard consequences and risk calculation. Bull. Volcanol. 67, 340–349.

Mahmood, A., Wolpert, R., Pitman, E., 2015. A physics-based emulator for the simulation of geophysical mass flows. SIAM/ASA J. Uncertain. Quantification 3, 562–585.

Marzocchi, W., Garcia-Aristizabal, A., Gasparini, P., Mastellone, M.L., Di Ruocco, A., 2012. Basic principles of multi-risk assessment: a case study in Italy. Nat. Hazards 62, 551–573.

Marzocchi, W., Sandri, L., Selva, J., 2008. BET_EF: a probabilistic tool for long- and short-term eruption forecasting. Bull. Volcanol. 70, 623–632.

Marzocchi, W., Woo, G., 2007. Probabilistic eruption forecasting and the call for an evacuation. Geophys. Res. Lett. 34.

Marzocchi, W., Zaccarelli, L., 2006. A quantitative model for the time-size distribution of eruptions. J. Geophys. Res. Solid Earth 111, B04204.

Mead, S.R., Magill, C.R., 2017. Probabilistic hazard modelling of rain-triggered lahars. J. Appl. Volcanol. 6, 8.

Mendoza-Rosas, A.T., De la Cruz-Reyna, S., 2008. A statistical method linking geological and historical eruption time series for volcanic hazard estimations: applications to active polygenetic volcanoes. J. Volcanol. Geoth. Res. 176, 277–290.

Mulargia, F., Gasperini, P., Tinti, S., 1987. Identifying different regimes in eruptive activity: an application to Etna volcano. J. Volcanol. Geoth. Res. 34, 89–106.

Nadejda, K., Anna, S., Alexander, G.-A., Daniel, M., Kevin, F., 2016. Multi-risk approach and urban resilience. Int. J. Disaster Resilience. Built. Environ. 7, 114–132.

Neall, V., Stewart, R., Smith, I., 1986. History and Petrology of the Taranaki Volcanoes, vol. 23. Royal Society of New Zealand Bulletin, pp. 251–263.

Neall, V.E., 1979. Geological Map of New Zealand: Sheets P19, P20, & P21: New Plymouth, Egmont, and Manaia. Department of Scientific and Industrial Research.

Newhall, C., Hoblitt, R., 2002. Constructing event trees for volcanic crises. Bull. Volcanol. 64, 3–20.

Ogburn, S.E., Calder, E.S., 2017. The relative effectiveness of empirical and physical models for simulating the dense undercurrent of pyroclastic flows under different emplacement conditions. Front. Earth Sci. 5.

Ogburn, S.E., Loughlin, S.C., Calder, E.S., 2015. The association of lava dome growth with major explosive activity (VEI $\geq$ 4): DomeHaz, a global dataset. Bull. Volcanol. 77, 40.

Paciorek, C.J., Schervish, M.J., 2004. Nonstationary covariance functions for Gaussian process regression. Adv. Neural Inf. Process. Syst. 273–280.

Pareschi, M., 2000. GIS and volcanic risk assessment. Nat. Hazards 21, 361–379.

Patra, A., Bevilacqua, A., Akhavan-Safaei, A., Pitman, E.B., Bursik, M., Hyman, D., 2020. Comparative analysis of the structures and outcomes of geophysical flow models and modeling assumptions using uncertainty quantification. Front. Earth Sci. 8.

Patra, A.K., Bauer, A.C., Nichita, C.C., Pitman, E.B., Sheridan, M.F., Bursik, M., Rupp, B., Webber, A., Stinton, A.J., Namikawa, L.M., Renschler, C.S., 2005. Parallel adaptive numerical simulation of dry avalanches over natural terrain. J. Volcanol. Geoth. Res. 139, 1–21.

Pitman, E.B., Nichita, C.C., Patra, A., Bauer, A., Sheridan, M., Bursik, M., 2003. Computing granular avalanches and landslides. Phys. Fluids 15, 3638–3646.

Platz, T., 2007. Understanding Aspects of Andesitic Dome-Forming Eruptions through the Last 1000 Yrs of Volcanism at Mt. Taranaki, New Zealand : a Dissertation Presented in Partial Fulfilment of the Requirements for the Degree of Doctor of Philosophy in Earth Science. Massey University, Palmerston North, New Zealand (Massey University.

Platz, T., Cronin, S.J., Cashman, K.V., Stewart, R.B., Smith, I.E.M., 2007. Transition from effusive to explosive phases in andesite eruptions — a case-study from the AD1655 eruption of Mt. Taranaki, New Zealand. J. Volcanol. Geoth. Res. 161, 15–34.

Platz, T., Cronin, S.J., Procter, J.N., Neall, V.E., Foley, S.F., 2012. Non-explosive, dome-forming eruptions at Mt. Taranaki, New Zealand. Geomorphology 136, 15–30.

Procter, J., Cronin, S., Platz, T., Patra, A., Dalbey, K., Sheridan, M., Neall, V., 2010. Mapping block-and-ash flow hazards based on Titan 2D simulations: a case study from Mt. Taranaki, NZ. Nat. Hazards. 53, 483–501.

Procter, J.N., Zernack, A.V., Cronin, S.J., 2021. Computer simulation of a volcanic debris avalanche from Mt. Taranaki, New Zealand. In: Roverato, M., Dufresne, A., Procter, J. (Eds.), Volcanic Debris Avalanches: from Collapse to Hazard. Springer International Publishing, Cham, pp. 281–310.

Pudasaini, S.P., 2012. A general two-phase debris flow model. J. Geophys. Res.: Earth Surf. 117.

Pudasaini, S.P., Miller, S.A., 2013. The hypermobility of huge landslides and avalanches. Eng. Geol. 157, 124–132.

Rasmussen, C., Williams, C., 2006. Gaussian Processes for Machine Learning. The MIT Press, Cambridge, Massachusetts, p. 266.

Rhoades, D.A., Dowrick, D.J., Wilson, C.J.N., 2002. Volcanic hazard in New Zealand: scaling and attenuation relations for tephra fall deposits from taupo volcano. Nat. Hazards 26, 147–174.

Rutarindwa, R., Spiller, E.T., Bevilacqua, A., Bursik, M.I., Patra, A.K., 2019. Dynamic probabilistic hazard mapping in the long valley volcanic region CA: integrating vent opening maps and statistical surrogates of physical models of pyroclastic density currents. J. Geophys. Res. Solid Earth 124, 9600–9621.

Sacks, J., Welch, W.J., Mitchell, T.J., Wynn, H.P., 1989. Design and analysis of computer experiments. Stat. Sci. 4, 409–423.

Sandri, L., Jolly, G., Lindsay, J., Howe, T., Marzocchi, W., 2012. Combining long- and short-term probabilistic volcanic hazard assessment with cost-benefit analysis to support decision making in a volcanic crisis from the Auckland Volcanic Field, New Zealand. Bull. Volcanol. 74, 705–723.

Santner, T.J., Williams, B.J., Notz, W., Williams, B.J., 2003. The Design and Analysis of Computer Experiments. Springer.

Sheridan, M.F., Stinton, A.J., Patra, A., Pitman, E.B., Bauer, A., Nichita, C.C., 2005. Evaluating Titan2D mass-flow model using the 1963 little tahoma peak avalanches, Mount rainier, Washington. J. Volcanol. Geoth. Res. 139, 89–102.

Snelson, E., Ghahramani, Z., Rasmussen, C.E., 2004. Warped Gaussian processes. Adv. Neural Inf. Process. Syst. 337–344.

Snoek, J., Swersky, K., Zemel, R., Adams, R., 2014. Input Warping for Bayesian Optimization of Non-stationary Functions. International Conference on Machine Learning, pp. 1674–1682.

Spiller, E., Bayarri, M., Berger, J., Calder, E., Patra, A., Pitman, E., Wolpert, R., 2014. Automating emulator construction for geophysical hazard maps. SIAM/ASA J. Uncertain. Quantification 2, 126–152.

Stefanescu, E.R., Bursik, M., Cordoba, G., Dalbey, K., Jones, M.D., Patra, A.K., Pieri, D.C., Pitman, E.B., Sheridan, M.F., 2012a. Digital elevation model uncertainty and hazard analysis using a geophysical flow model. Proc. Math. Phys. Eng. Sci. 468, 1543.

Stefanescu, E.R., Bursik, M., Patra, A.K., 2012b. Effect of digital elevation model on Mohr-Coulomb geophysical flow model output. Nat. Hazards 62, 635–656.

Stevens, N.F., Manville, V., Heron, D.W., 2003. The sensitivity of a volcanic flow model to digital elevation model accuracy: experiments with digitised map contours and interferometric SAR at Ruapehu and Taranaki volcanoes, New Zealand. J. Volcanol. Geoth. Res. 119, 89–105.

Stirling, M., Bebbington, M., Brenna, M., Cronin, S., Christophersen, A., Deligne, N., Hurst, T., Jolly, A., Jolly, G., Kennedy, B., Kereszturi, G., Lindsay, J., Neall, V., Procter, J., Rhoades, D., Scott, B., Shane, P., Smith, I., Smith, R., Wang, T., White, J. D.L., Wilson, C.J.N., Wilson, T., 2017. Conceptual development of a national volcanic hazard model for New Zealand. Front. Earth Sci. 5.

Stirling, M., Wilson, C., 2002. Development of a volcanic hazard model for New Zealand: first approaches from the methods of probabilistic seismic hazard analysis. Bull. N. Z. Soc. Earthq. Eng. 35, 266–277.

Torres-Orozco, R., Cronin, S.J., Damaschke, M., Pardo, N., 2017a. Diverse dynamics of holocene mafic-intermediate plinian eruptions at Mt. Taranaki (Egmont), New Zealand. Bull. Volcanol. 79, 76.

Torres-Orozco, R., Cronin, S.J., Pardo, N., Palmer, A.S., 2017b. New insights into Holocene eruption episodes from proximal deposit sequences at Mt. Taranaki (Egmont), New Zealand. Bull. Volcanol. 79, 3.

Vehtari, A., Mononen, T., Tolvanen, V., Sivula, T., Winther, O., 2016. Bayesian leave-one-out cross-validation approximations for Gaussian latent variable models. J. Mach. Learn. Res. 17, 3581–3618.

Wang, T., Bebbington, M., 2012. Estimating the likelihood of an eruption from a volcano with missing onsets in its record. J. Volcanol. Geoth. Res. 243–244, 14–23.

Wilson, T.M., Stewart, C., Sword-Daniels, V., Leonard, G.S., Johnston, D.M., Cole, J.W., Wardman, J., Wilson, G., Barnard, S.T., 2012. Volcanic ash impacts on critical infrastructure. Phys. Chem. Earth 45–46, 5–23. Parts A/B/C.

Wolpert, R.L., Spiller, E.T., Calder, E.S., 2018. Dynamic statistical models for pyroclastic density current generation at soufrière hills volcano. Front. Earth Sci. 6.

Zernack, A.V., Procter, J.N., 2021. Cyclic growth and destruction of volcanoes. In: Roverato, M., Dufresne, A., Procter, J. (Eds.), Volcanic Debris Avalanches: from Collapse to Hazard. Springer International Publishing, Cham, pp. 311–355.

Zernack, A.V., Procter, J.N., Cronin, S.J., 2009. Sedimentary signatures of cyclic growth and destruction of stratovolcanoes: a case study from Mt. Taranaki, New Zealand. Sediment. Geol. 220, 288–305.